UNIVERSITY OF CALIFORNIA SAN DIEGO

Plasma Mirror Focal Spot Quality for Glass and Aluminum Mirrors for LASER Pulses up to 20 picoseconds

A thesis submitted in partial satisfaction of the
requirements for the degree Master of Science

in

Engineering Sciences (Engineering Physics)

by

Brandon Christian Edghill

Committee in charge:

Professor Farhat N. Beg, Chair
Professor Nicholas S. Boechler
Professor Javier E. Garay

2019

The Thesis of Brandon Christian Edghill is approved, and it is acceptable in quality and form for publication on microfilm and electronically:

Chair

University of California San Diego

2019

DEDICATION

To my family for supporting me through the hard times and helped celebrate the good.

TABLE OF CONTENTS

LIST OF FIGURES

ACKNOWLEDGEMENTS

I would like to acknowledge Professor Farhat N. Beg for his support as the chair of my committee and the many drafts it took to get the paper ready for publication.

I would also like to specially thank Dr. Pierre Forestier-Colleoni whose guidance was pivotal in getting this far. Without his patience I would still be far off from completion.

Thank you to all the co-authors,Pierre Forestier-Colleoni, Jaebum Park, Alexander Rubenchik, Farhat N. Beg and Tammy Ma, who took the time to help improve this work to what it is today.

Chapter 4, in part is currently being prepared for submission for publication of the material. Brandon Edghill, Pierre Forestier-Colleoni, Jaebum Park, Alexander Rubenchik, Farhat N. Beg and Tammy Ma. The thesis author was the primary investigator and author of this material.

Chapter 5, in part is currently being prepared for submission for publication of the material. Brandon Edghill, Pierre Forestier-Colleoni, Jaebum Park, Alexander Rubenchik, Farhat N. Beg and Tammy Ma. The thesis author was the primary investigator and author of this material.

This work was performed under the auspices of the Department of Energy by Lawrence Livermore National Laboratory through grant LDRD 17-ERD-039. LLNL-POST-760824

Lastly I would like to thank my partner, Andy Snitovsky, who was truly a pillar of support throughout this experience, without whom this achievement would mean little.

ABSTRACT OF THE THESIS

Plasma Mirror Focal Spot Quality for Glass and Aluminum Mirrors for LASER Pulses up to 20 picoseconds

by

Brandon Christian Edghill

Master of Science in Engineering Sciences (Engineering Physics)

University of California San Diego, 2019

Professor Farhat N. Beg, Chair

High intensity short pulse lasers are being pushed further as applications continue to demand higher laser intensities. Uses such as radiography and laser-driven particle acceleration require these higher intensities to produce the necessary x-ray and particle fluxes. Achieving these intensities however is limited by the damage threshold of costly optics and the complexity of target chambers. This is evidenced by the Advanced Radiographic Capability (ARC) short pulse laser, at the National Ignition Facility (NIF) at the Lawrence Livermore National Laboratory, producing four high energy $\approx$1 kJ laser pulses at 30 ps pulse duration being limited to an intensity of 10^{18} W/cm^2 by the large focal spot size of $\approx 100\ \mu$m. Due to the setup complexity of NIF,

changing the location of the final focusing parabola in order to improve the focal spot size is not an option. This leads to the possible use of disposable ellipsoidal plasma mirrors (PMs) placed within the chamber, close to the target in an attempt to refocus the four ARC beams. However, the behavior of plasma mirrors at these relatively long pulse durations (tens of ps) is not well characterized. The results from the COMET laser at the Jupiter Laser Facility (JLF) carried out at 0.5 to 20 ps pulse durations on flat mirrors are presented as a necessary first step towards focusing curved mirrors. The data shows defocusing at longer pulse durations and higher intensities, with less degradation when using aluminum coated mirrors.

Introduction

The Light Amplification by Stimulated Emission of Radiation, or LASER for short, has woven its way into many aspects of modern society while remaining relatively hidden. They are used in medicine for cancer treatments and are responsible for the production of all computer CPUs and GPUs that people have grown accustom to using in their daily lives. This has lead to a multi-billion dollar industry spread across mainstream tech, military applications and science.

The technique/phenomenon responsible for the laser is called stimulated emission and it was first theorized by Albert Einstein in a 1917 paper, ”On the Quantum Theory of Radiation”. It was not until the 1950’s that it was conceptualized that this could be used to amplify electromagnetic radiation by Charles Townes (1951). This, together with the collective work of Nikolai Basov and Alexander Prokhorov on negative absorption (pumping method) and quantum electronics lead to oscillators and amplifiers based on the maser-laser principle for which they were awarded the 1964 Nobel Prize. In 1959 the acronym LASER was first coined by Gordon Gould and in 1960 the first LASER was constructed by Theodore Maiman.

As LASERs uses in both commercial and scientific realms expanded there has been significant progress in terms of improving their capabilities. Particularly in scientific study the need for higher and higher intensities grows as it is needed to probe new regimes and expand our understanding. To achieve these high intensities a method called Chirped Pulse Amplification (CPA) is used. This method was discovered by Donna Strickland and Gérard Mourou in 1985 who were later awarded the Physics Nobel Prize in 2018 for their impact on the scientific community allowing the achievement of extremely high power (TeraWatt). The workings of this method will be explored in Chapter 1. However, while this amplification method allowed

for large improvements in achievable intensity, it also suffers from LASER problems such as the pedestal which is a result of spontaneous emission (also discussed by Einstein in the same paper as stimulated emission). This pedestal can be above the damage threshold of a material interacting with the target before the main pulse, ionizing it, making it difficult to know the conditions under which the target interacted with the main pulse. To combat this problem, plasma shuttering, also called Plasma Mirrors, has been developed.

Plasma mirrors clean the pulse by allowing the pedestal to be transmitted (up to 99%) before the ionizing and reflecting the main pulse towards the target. This has been well studied in the ultra-short regime (femtosecond to one picosecond). As the demands for higher intensity LASERs grow ellipsoidal plasma mirrors have been utilized to increase LASER intensities by refocusing the main pulse. They act as disposable refocusing optics in lieu of another multi-thousand dollar optic as used in the primary focusing. The primary focusing optics ability to focus the LASER are currently limited by the damage threshold ($\approx 1\ Jcm^{-2}$) and high cost. The relatively low cost nature of plasma mirrors allows them to be placed closer to the focal spot past the damage threshold acting as a disposable optic to achieve a higher final intensity on target.

This thesis goes into the details and results of an experiment carried out at the COMET LASER facility at Lawrence Livermore National Laboratory. Flat plasma mirrors were tested in the multi-picosecond regime to see how they respond to the longer pulse durations ($>$1 ps). This was done as a first step towards the use of ellipsoidal plasma mirrors on multi-picosecond LASERs. Two materials were tested, the traditional glass mirror (SiO_2) and aluminum (Al) coated mirrors to see the effects of a change in material. The far field of the LASER after interacting with the mirrors was captured, analyzed and compared for varying laser intensities and pulse durations. These results are presented after exploring the background theory and concepts involved.

Chapter 1

High Powered LASERs

The laser of today represents the technological improvements and methodologies developed to enhance the principal first theorised by Einstein called stimulated emission. To understand this we first look at the process known as spontaneous emission. This is the quantum process that sees the electromagnetic field consisting of packets called photons. Consider an arbitrary molecule that has two of these fixed energy levels, ε_m and ε_n where $\varepsilon_m > \varepsilon_n$. Without external stimulation there can be a transition from state Z_m to Z_n by emitting a photon of energy $\varepsilon_m - \varepsilon_n$ and frequency ν. The number of light sources in this excited state at a time t is given by $N(t)$ and its decay rate or emission rate is expressed as:

$$\frac{\partial N(t)}{\partial t} = -A_{21}N(t), \tag{1.1}$$

where A_{21} is the rate of spontaneous emission unique to this characteristic of indices considered. In the case of stimulated emission an external electric field, such as a beam of light, can induce an emission where a photon will be emitted of the same frequency and phase. For a group of such molecules the rate of this stimulated emission can be expressed as:

$$\frac{\partial N_2}{\partial t} = -\frac{\partial N_1}{\partial t} = -B_{21}\rho(\nu)N_2, \tag{1.2}$$

where B_{21} is a proportionality constant for that particular transition and $\rho(\nu)$ is the radiation density of the incident field at frequency ν. Therefore the emission rate is proportional

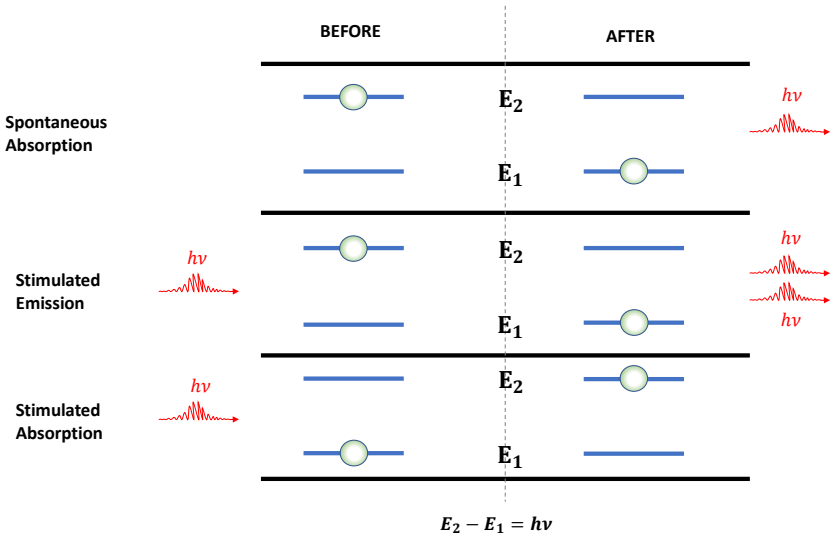

Figure 1.1. Figure showing spontaneous emission, stimulated emission and absorption.

to the number of atoms in the excited Z_2 state given by N_2. Similar to the stimulated emission process there is the atomic absorption process which is essentially the reverse. This is expressed as:

$$\frac{\partial N_2}{\partial t} = -\frac{\partial N_1}{\partial t} = -B_{12}\rho(\nu)N_1, \tag{1.3}$$

where B_{12} is the proportionality constant for that particular transition. These three processes are summarized visually in Figure 1.1.

It was shown by Einstein that the relation $B_{12} = B_{21}$ and as such the net rate of stimulated absorption to emission depends on the difference in population of the states. This means if N_2 can be artificially augmented so that the rate of stimulated emission exceeds the rate of absorption + losses of the system then the laser threshold is exceeded and the light can be amplified. To this end Alfred Kastler developed a method called optical pumping in 1950 which he was awarded a Nobel prize in 1966 [1]. A gain medium is pumped via a light source which excites the electron to a higher energy level. However there must be at least 3 stages for population inversion to occur in order to prevent the pumping source from causing stimulated emission. So this 3-stage process

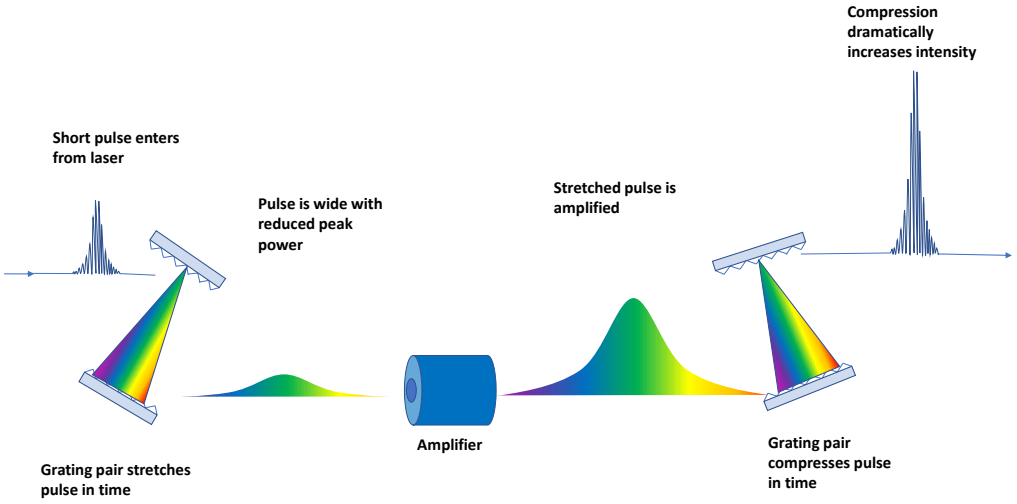

Figure 1.2. Schematic showing the Chirped Pulse Amplification process.

must then decay to a slightly lower energy level than the one it was excited to. This prevents stimulated emission by the pumping source and allows stimulated emission via the main laser. This takes place inside a optical resonator or cavity which allows the light to circulate for several passes allowing a larger total amplification. The amplified beam is then directed to an output coupler which lets a small part of the beam through. This is the basic operation of a LASER.

Since the first operational laser in 1960, scientist have pushed for higher and higher intensities in order to open up new areas of research. General progress in laser intensities came in the form of Q-switching in early 1960's achieving higher energies, longer pulse durations and lower repetition rates compared to mode-locking and Mode-locking in 1965 achieving ultra short pulse durations $10^{-10-18}s$ pushing the probeable regimes further, achieving Mega-Watt and Giga-Watt powers respectively. Progress on increasing laser intensity stagnated as laser pulses became limited by the damage thresholds of materials and the non-linear effects introduced just below this threshold. This meant that with current techniques achieving higher intensities would destroy optics in the beamline. It was not until 1985 when the chirped pulse amplification method (CPA) was developed pushing the achievable intensities further by partially circumventing the limits of the old methods.

The summary of this method can be seen in Figure 1.2. A short laser pulse is first stretched using two gratings to stretch the pulse in time prior to entering the gain medium. The gratings cause the low frequency component of the pulse to travel a shorter path than the high frequency component via dispersion. This positively chirps the pulse stretching it upwards of 1000 $\times$. This stretched pulse is then amplified via the gain medium without exceeding the damage threshold. Lastly the pulse is re-compressed through the reversed process used to initially stretch it. This compresses all the energy back into a short pulse leading to very high peak intensities.

Chapter 2

Plasma Physics

The high intensity lasers referenced in this thesis convert matter from the solid state to what is commonly referred to as the fourth state of matter: plasma. This is done by ionizing the target and freeing the electrons from their bound states. The different ways this can occur will be explored in this chapter. Furthermore, the basic characteristics of a plasma that differentiate it from solids, liquids and gases will also be explored, namely their collective behaviour. This collective nature greatly complicates the physics involved as individual charged particles exert effects to many charged particles around it. This nature is explored along with the interactions a laser has with a plasma.

2.1 Plasmas

Plasmas arise from the ionization of a material and the way this occurs will be discussed later. Here we move forward with the assumption that the ionization has already occurred and a plasma has been created. Plasmas have key properties [12, 5] :

1) Quasi-Neutrality

2) Collective Behaviour

Quasi-neutrality refers to a plasma that is, as a whole, neutral. What this means is that the free electrons and ions that the plasma consists of approximately balance each other out

charge-wise to form an equilibrium. This is mathematically expressed as:

$$n_e \simeq Z n_i. \tag{2.1}$$

Collective behaviour results from the long-range nature of electric potentials as it only falls off at a rate of $1/r$. This causes plasmas to behave differently to regular gases which consist of charge neutral molecules. For a gas the particle collisions would dominate and dictate the motion of the fluid whereas in a plasma the far-reaching Coulomb potential of the charged particles affects all the other charged particles in the plasma. Therefore this collective behaviour is when the ionized fluid's movement is dominated by the sum total effects of the charged particles/regions instead of localized particle collisions. This also holds true for short lived microscopic charge fluctuations which are quickly neutralised by the plasma allowing long term macroscopic fields to be the primary governing factor.

Before exploring the criteria needed to meet these two attributes of a plasma and how exactly charge fluctuations can become shielded, collisions, the temperature and particle distribution/density in how they apply to plasmas needs to be examined. The following are adapted from Intro to Plasma Physics notes [12] and Introduction to Plasma Physics and Controlled Fusion [5]. For simplicity, motion is examined in one direction. Considering a gas in thermal equilibrium, the particles can be expressed by the Maxwellian probability distribution:

$$f(u) = A exp\left(-\frac{1}{2}\frac{mu^2}{k_B T}\right), \tag{2.2}$$

where $f(u)$ is the number of particles of energy u, $1/2mu^2$ is the kinetic energy and k_B is the Boltzman's constant. The particle density can then be expressed as the integral of Eq. 2.2 with respect to u giving:

$$n = A\left(\frac{m}{2\pi k_B T}\right)^{-1/2}. \tag{2.3}$$

This results in a gaussian with a width characterized by T which is ubiquitously called temperature. Averaging the kinetic energy for our system we find the following relation:

$$E_a v = \frac{1}{2} k_B T \text{ per degree of freedom.} \tag{2.4}$$

This means for three dimensional space the average kinetic energy is $3/2 k_B T$. This close relationship between energy and temperature has lead to temperature being referenced as an energy:

$$k_B T = 1 \; eV,$$
$$1 \; eV \approx 11600 \; K.$$

Next is the concept of Debye Shielding. This phenomena arises due to the free charge particles available in a plasma. The most common example of this is to introduce an electric field into the plasma via two charged spheres (each of opposite charge). In response, the free electrons gather to neutralise the positively charged sphere and the ions neutralise the negatively charged sphere acting to screen the electric fields generated by the two charged spheres neutralising them completely. However as the thermalized plasma consists of ions and electrons of the same energy the heavy ions remain relatively motionless while the lighter electrons are fast and escape at the edge of the neutralising cloud before being recaptured by the field causing the shielding to be incomplete. This allows potentials on the order of $K_B T / e$ to leak through. The scale length on which this occurs depends equally on the plasma's temperature and density (primarily electron density as ions are approximately stationary on electron time scales). This scale length is called the Debye length and is expressed as:

$$\lambda_D = \left(\frac{\varepsilon_0 k_B T_e}{e^2 n_e} \right)^{1/2}. \tag{2.5}$$

With the number of particles contained within the Debye Sphere given as:

$$N_D = \frac{4}{3} n \pi \lambda_D^3. \tag{2.6}$$

The last factor needed in order to determine if the conditions of a plasma are met is the electron plasma frequency (electrons typically dominate motion due to ions larger mass). This quantity is expressed as:

$$\omega_p = \left(\frac{e^2 n_e}{\varepsilon_0 m_e} \right)^{1/2}. \tag{2.7}$$

With these quantities defined the three criteria of a plasma are met when:

1. $\lambda \ll L$
2. $N_D \ggg 1$
3. $\omega\tau > 1$

Condition 1 and 2 are required for collective behaviour as the plasma must be significantly larger than the Debye sphere for shielding to have an effect and the number of particles inside the Debye sphere must be large enough to provide the shielding. Condition 3, where τ is the average time between collisions with a neutral atom, ensures that motion is controlled by the fields and motions of charged particles and not dominated by neutral collisions typical of regular gases.

2.2 Electromagnetic Wave Propagation in Plasmas

Electromagnetic wave propagation inside a plasma is dictated by Maxwell's equations. These well known equations take the following form in a plasma [16]:

$$\nabla \cdot \mathbf{D} = 4\pi\rho, \tag{2.8}$$

$$\nabla \cdot \mathbf{B} = 0, \tag{2.9}$$

$$\nabla \times \mathbf{E} = -\frac{1}{c}\frac{\partial \mathbf{B}}{\partial t}, \tag{2.10}$$

$$\nabla \times \mathbf{H} = \frac{1}{c}\left(4\pi\mathbf{J} + \frac{\partial \mathbf{D}}{\partial t}\right), \tag{2.11}$$

expressed with the Gaussian unit convention where $\mathbf{D} = \varepsilon\mathbf{E}$ and $\mathbf{B} = \mu\mathbf{H}$ where ν is the magnetic permeability. These reduce to the more common form of Maxwell's equations in a vacuum. Solutions can be found using assumptions to simplify the math such as no large external magnetic fields. Looking at a linearized plasma responding to a laser field with high frequency we get:

$$\mathbf{E} = \mathbf{E}_\mathbf{x} e^{(-i\omega t)}, \tag{2.12}$$

$$\mathbf{B} = \mathbf{B}_\mathbf{x} e^{(-i\omega t)}. \tag{2.13}$$

The assumption of the laser field being high (i.e. greater than the plasma frequency) allows the treatment of the ions as stationary. Further more assuming small oscillations we can neglect products of motion and motion or motion and magnetic field, in other words keeping first order approximations. Substituting in the fields from Eq. 2.12 and Eq. 2.13 and taking the curls of Eq. 2.10 and Eq. 2.11 you get the wave equations for electric and magnetic fields as:

$$\nabla^2\mathbf{E} - \nabla(\nabla \cdot \mathbf{E}) + \frac{\omega^2}{c^2}\varepsilon\mathbf{E} = 0, \tag{2.14}$$

$$\nabla^2\mathbf{B} + \frac{\omega^2}{c^2}\varepsilon\mathbf{B} + \frac{1}{\varepsilon} \times (\nabla \times \mathbf{B}) = 0. \tag{2.15}$$

As a simple example of how this dictates laser propagation in a plasma let us consider a plasma of uniform density. This results in $\nabla\varepsilon = 0$ and $\nabla \cdot \mathbf{E} = 0$ whcih makes the wave equation for both electric and magnetic fields (Eq. 2.14 and Eq. 2.15) the same. For a spatial distribution of $exp\,(i\mathbf{k}\cdot\mathbf{x})$ the electromagnetic dispersion relation inside the plasma becomes:

$$c^2k^2 = \omega^2 - \omega_{pe}^2, \tag{2.16}$$

where ω is the laser frequency. From Eq. 2.16 it can be seen that as the laser frequency is approached by the plasma frequency and is finally exceeded by it1054 c the wave number becomes imaginary. This means that the laser propagate in an imaginary direction or in other words it does not propagate further in space. As the frequency of a laser is relatively constant and the properties of the plasma change as they interact with the laser field the plasma frequency changes. In this case once the plasma frequency equals the laser frequency then the plasma becomes opaque to the laser. This results in two regimes, $\omega > \omega_p$ being underdense plasma and $\omega_p > \omega$ being overdense plasma. By substituting the turning point from underdense to overdense plasma into Eq. 2.7 we get what is called the critical density of electrons which bars laser propagation in a plasma as:

$$n_{cr} = \frac{m_e\varepsilon_0}{e^2}\omega^2. \tag{2.17}$$

The point that this occurs also has a dependency on the laser's incident angle. For s-polarized light with an angle of incidence θ the more general electron density needed for reflection is expressed as:

$$n_e = n_{cr}cos^2\theta, \tag{2.18}$$

which is lower than or equal to n_{cr} for any angle. This opaque limit is what makes the plasma highly reflective and leads to the fundamental principle of plasma mirrors which will be

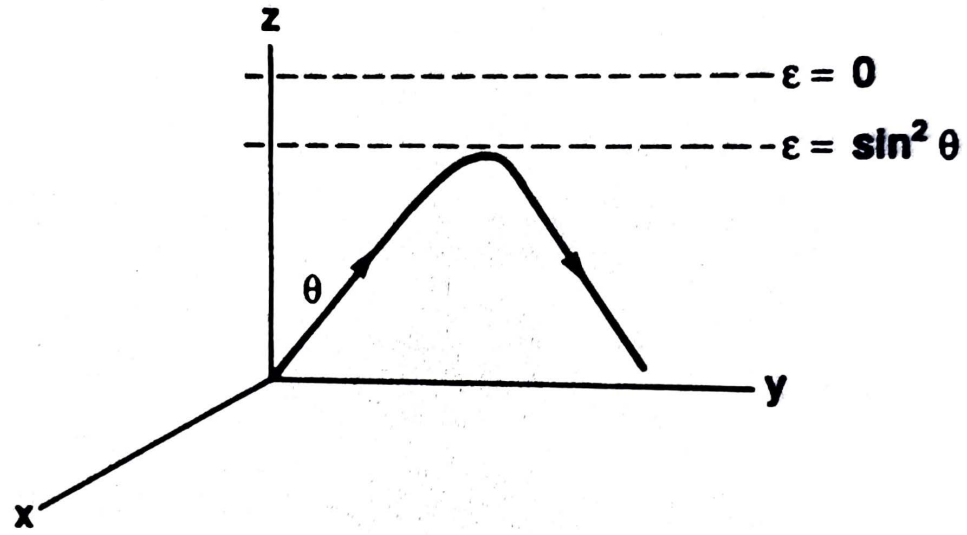

Figure 2.1. Figure showing an example of an electromagnetic wave obliquely incident on an inhomogenous plasma. Adapted from Kruer [21]

explored later in Chapter 2.3.

As the basics of a plasma and how it propagates has been explored, it is paramount that we explore the means by which the laser's energy is able to couple to the plasma. There are several laser plasma absorption mechanisms that take place and their dominance varies based on both laser and plasma conditions [21, 13, 25].

2.2.1 Resonant Absorption

The resonant absorption mechanism appears close to the critical density of a plasma (2.17) for p-polarized light only. It occurs as the electromagnetic wave couples with the plasma density due to a component of the electric field being along the density gradient. This component causes electrostatic oscillations that are resonantly enhanced by the plasma.

Consider an inhomogeneous plasma of density $n_e(z)$ with an incident plane electromagnetic wave of direction $\vec{k} = \vec{y} + \vec{z}$ defined by angle θ shown in Fig. 2.1. The laser's electric field is given by $\mathbf{E} = E_y\hat{y} + E_z\hat{z}$ leading to a poisson's equation of:

$$\nabla \cdot (\varepsilon \mathbf{E}) = 0 = \varepsilon \nabla \cdot \mathbf{E} + \nabla \varepsilon \cdot \mathbf{E}. \tag{2.19}$$

However as the dielectric function is only a component in the density direction of the plasma, $\varepsilon(z) = 1 - \frac{\omega_{pe}^2(z)}{\omega^2}$, Eq. 2.19 reduces to:

$$\nabla \cdot \mathbf{E} = -\frac{1}{\varepsilon}\frac{\partial \varepsilon}{\partial z} E_z. \tag{2.20}$$

What becomes clear from looking at Eq. 2.20 is that a resonance will occur as ε tends to 0. Now looking at the dielectric equation for the plasma means this occurs at $\omega_{pe} = \omega$, i.e. the critical surface (Eq. 2.17). This tells us that for a plasma with a non-uniform charge density any laser field will cause charge separation but at the surface where the plasma frequency and laser frequency match the plasma resonantly responds enhancing this charge separation and greatly exciting the electrons. Though the laser is reflected at this point its fields diffuse in the plasma creating an evanescent wave past the critical density which decreases exponentially. Here the particles are accelerated but due to the decreasing field the restoring force is weaker so the particles keep some of the energy imparted to them.

Resonant absorption varies based on both incident angle and the scale length of the plasma gradient. For an incident angle θ and scale length defining a linear density by $L = \frac{n_{cr}}{n_e} z$ the driver field for resonant absorption can be seen to vary based on the following variable[21]:

$$\phi \simeq 2.3 sin\theta \left(\frac{\omega L}{c}\right)^{1/3} e^{-\frac{2\omega L}{3c} sin^3\theta}. \tag{2.21}$$

This means that for small angles the driver field is reduced to 0 and for long plasma gradients the driver field is diminished as the electric field has too far to tunnel through to reach the critical density surface. This leads to a fractional absorption of:

$$f_A \simeq \frac{1}{2}\phi^2. \tag{2.22}$$

This was found to be in good agreement with the numerical solution found by Denisov [9].

2.2.2 Vacuum Heating

Resonant absorption was shown to fall off for plasma density scale lengths that were too long in Eq. 2.22 but the same can be said for density gradients that are too steep. This results in an L value that cannot support the resonant wave leading to the special case of resonant absorption called vacuum heating. This scaling is expressed as:

$$x_{res} \simeq \frac{eE_L}{m_e\omega^2} = \frac{v_{os}}{\omega}, \tag{2.23}$$

where x_{res} is the amplitude of the resonant wave. If this factor exceeds the density scale length L then the plasma is no longer able to support the plasma oscillations. However at this point a different mechanism begins to take place called the Brunel mechanism or Vacuum heating. Here electrons near the plasma-vacuum boundary experience the laser field directly. With a steep plasma density scale length can be pulled out into the vacuum by the laser field past the range of the Debye thermal sheath $\lambda_D = v_{te}/\omega_p$. At this point the laser field reverses, accelerating the electron towards the plasma. However due to the steep density profile the laser field cannot propagate deep into the plasma as n_{cr} is close to the plasma surface. Therefore the laser field can only penetrate to the skin depth of c/ω_p. This allows the electron to continue inward in the plasma with no decelerating laser field to pull it back. Eventually the electron loses its energy due to collisions causing the electrons energy to be transferred to the plasma.

Brunel developed an analytic model based on the capacitor approximation [3]. Here the magnetic field component of the wave is neglected and assumes that the laser has an oblique incidence, i.e. has a component of the electric field normal to the target surface. This field sets

up a standing wave:

$$E_d = 2E_L sing\theta, \tag{2.24}$$

where theta is the angle of incidence and E_L is the laser's field. This pulls electrons from the surface into the vacuum at a distance of $\triangle x$ creating a surface number density similar to a capacitor given by $\Sigma = n_e \triangle x$. The sheet generates a field of:

$$\triangle E = 4\pi e\Sigma. \tag{2.25}$$

Σ is then found by equating the driving field to the sheet field (Eq. 2.25) giving the result of $\Sigma = \frac{2E_L sin\theta}{4\pi e}$. As the sheet electrons return to their rest position they acquire a velocity of $v_d \simeq 2v_{os} sin\theta$ where v_{os} is the electron quiver velocity in a laser field. Moving forward with the assumption that 100% of the electrons are retained/stuck by the solid then the average energy density deposited per laser cycle is:

$$P_a = \frac{\sigma}{\tau}\frac{mv_d^2}{2} \simeq \frac{1}{16\pi^2}\frac{e}{m\omega}E_d^3, \tag{2.26}$$

where τ is the laser period. With an incoming laser power of $P_L = cE_L^2 cos\theta/8\pi$ one can substitute Eq. 2.24 to obtain the fraction absorption:

$$\eta \equiv \frac{P_a}{P_L} = \frac{4}{\pi}a_0\frac{sin^3\theta}{cos\theta}, \tag{2.27}$$

where $a_0 = v_{os}/c$. As $a_o^2 \propto I\lambda^2$, Eq. 2.27 tells us that absorption scales favourably with increasing incident angles and laser intensity. For high intensities and short scale lengths absorption theoretically saturates at around $10-15\%$ but for intermediate values of $I\lambda = 10^{16}$ Wcm$^{-2}\mu$m^2 and $L/\lambda \sim 0.1$ absorption can get as high as 70%.

2.2.3 Inverse Bremsstrahlung

Resonance absorption and vacuum heating dealt with collisionless means to transfer energy from the laser to the plasma. Inverse bremsstrahlung is a collisional means of transferring energy from the laser to the plasma. It is a result of an electron oscillating in the laser's electric field being scattered off of an ion. This dephases the electron from the electric field allowing it to escape with a net energy increase. If this interaction does not occur and the laser was turned off then the electron will end up with the same energy it had before the laser's field was there. What this means is that the scattering is a way in which an electron can hold on to some of the energy from half the laser's electric field cycle by using the ion to conserve momentum. The mathematical representation of this phenomenon is derived in [21], [14] and [13]. This derivation has been summarized in the following.

Starting with the assumption of small field amplitudes and non-relativistic response of the fluid we use Lorentz equation of motion for electrons in an electromagnetic field.

$$\frac{\partial \mathbf{v}}{\partial t} = -\left(\mathbf{E} + \frac{\mathbf{v}}{c} \times \mathbf{B}\right) \frac{e}{m} - m\nu_{ei}\mathbf{v}, \tag{2.28}$$

where ν_{ei} is the electron-ion collision frequency [21, 8] expressed as:

$$\nu_{ei} = \frac{4\,(2\pi)^{1/2}}{3} \frac{n_e Z e^4}{m^2 v_{te}^3} ln\Lambda, \tag{2.29}$$

where $ln\Lambda$ is the Coulomb logarithm which in simple terms is the ratio of the max distance between collisions (Debye sphere) to the smallest distance (atom). Taking the curl of the Faraday and Ampère equations the relevant electromagnetic wave equations are found. Following this it is assumed that the field and fluid quantities are harmonically time dependent to $\exp(-i\omega t)$ and then the equations are linearized. This removes the magnetic field as a factor and

reveals the solution to the electron velocity from Eq. 2.28 as:

$$v_e = \frac{-i}{\omega + i\nu_{ei}} \frac{e\mathbf{E}_1}{m}. \tag{2.30}$$

Eq. 2.30 leads to a current density:

$$\mathbf{J} = -en_0 v_1 = \frac{i\omega_{pe}^2}{4\pi(\omega + i\nu_{ei})}\mathbf{E} = \sigma\mathbf{E}, \tag{2.31}$$

where σ is the conductivity. Substituting Eq. 2.31 into the curl of Faraday's equation leads to:

$$\nabla^2\mathbf{E} + \frac{\omega^2}{c^2}\mathbf{E} = \frac{\omega_{pe}^2}{\omega c^2}\frac{\mathbf{E}}{(\omega + i\nu_{ei})} + \nabla(\nabla\cdot\mathbf{E}). \tag{2.32}$$

If we consider a spatially uniform plasma the electric field can be approximated as $\mathbf{E}(x) \sim e^{ik\cdot x}$ and ignoring fast oscillations (WKB approximation) Eq. 2.32 becomes:

$$\omega^2 = k^2c^2 + \omega_{pe}^2\left(1 - \frac{i\nu_{ei}}{\omega}\right), \tag{2.33}$$

where it was assumed that $\nu_{ei}/\omega \ll 1$. The laser's light wave is now damped where we can separate ω into real and imaginary parts $\omega = \omega_r - i\nu/2$. ν is the damping rate where:

$$\omega_r = \left(\omega_{pe}^2 + k^2c^2\right)^{1/2}, \tag{2.34}$$

$$\nu = \frac{\omega_{pe}^2}{\omega_{pe}^2 + k^2c^2}\nu_{ei}. \tag{2.35}$$

In the case where ω is real and k is complex you can divide the group velocity of the light wave (v_g) by the damping rate (ν) to recover the energy damping length. This leads to a

collisional absorption rate for a uniform plasma of length L as:

$$\eta = 1 - e^{-2\nu_g \nu L}. \tag{2.36}$$

For inhomogenous density profiles and oblique incidence the derivations become very involved[21] and the solution is expressed as:

$$\eta = 1 - e^{-\frac{32\nu_{ei}^* L}{15c}cos^5\theta}, \tag{2.37}$$

where θ is the angle of incidence of the laser to the plasma. It is important to note the importance of the density profile of the plasma as $\nu_{ei}^* = \nu_{ei} n_{cr}/n_e$. As a result for a exponentially varying density profile Eq. 2.37 becomes:

$$\eta = 1 - e^{-\frac{8\nu_{ei}^* L}{3c}cos^3\theta}. \tag{2.38}$$

From the derivations and final equations provided thus far it is important to note that inverse bremsstrahlung, or breaking radiation, is dominant further from the critical density and for long plasma gradients.

2.2.4 Ionization

Ionization is the broad term for any process that removes a bound electron from an atom/molecule. To do so the electron has to be given sufficient energy to break away from the atom. In other words this ionization energy must be equal to or greater than the potential energy of the bond holding the electron to the nucleus. As light is quantum in nature and consists of packets of energy called photons, if the frequency is high enough i.e. if the photon has enough energy it can strip an electron from the pull of the atom. If a single photon does not have enough energy then multiple photons can add up to provide the energy however this has a lower probability of occurring. In some cases more photons than are needed to ionize the atom can be

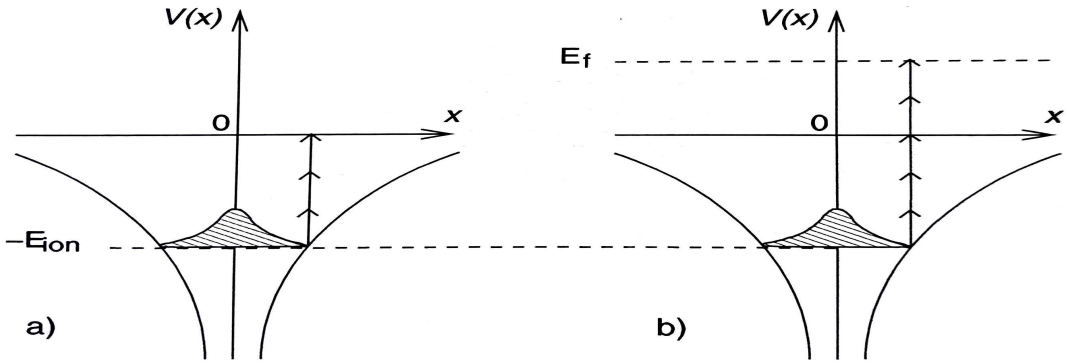

Figure 2.2. a) Schematic picture of multiphoton ionization (MPI). An electron with binding energy E_{ion} simultaneously absorbs n photons with energy $h\bar{\omega}$ and is subsequently released from the atom with minimal kinetic energy. b) Above-threshold ionization (ATI): the electron absorbs more photons than necessary for ionization, leaving the atom with significant momentum. Adapted from P. Gibbon [13]

absorbed leading to above threshold ionization (ATI) represented as follows:

$$E_f = (n+s)\hbar\omega_L - E_{ion}, \tag{2.39}$$

where n is the number of photons needed for multiphoton ionization, s is the excess number absorbed, ω_L is the laser angular frequency and E_{ion} is the energy needed to ionize the electron. This maintains momentum conservation by taking place in the field of the parent ion. Figure 2.2 shows a simple comparison of single and multiphoton ionization adapted from "Short Pulse Laser Interactions with Matter" [13].

The electron can also be ionized via a strong enough electric field. A baseline example can be constructed using the hydrogen atom. The following equations follow P. Gibbon's derivations [13]. The electric field strength experienced by the electron in orbit is:

$$E_a = \frac{e}{4\pi\varepsilon_0 a_B^2}, \tag{2.40}$$

where a_B is the Bohr radius. This provides the intensity I_a:

$$\begin{aligned} I_a &= \frac{\varepsilon_0 c E_a^2}{2} \\ &\approx 3.51 \times 10^{16} W cm^{-2}. \end{aligned} \tag{2.41}$$

A laser whose intensity is greater than I_a will surely ionize the hydrogen's electron via its field. However this intensity is not required to ionize an atom. It can be accomplished at lower intensities via multiphoton effects discussed earlier.

Of note is the controversy surrounding the multiphoton ionization theory where for higher energies the spectrum becomes dominated with peaks above $n\hbar\omega$ suggesting that ATI is non-perturbative (cannot be simplified down to an approximate simple formula). Perturbative multiphoton ionization's assumption that atomic binding energies are fixed in the laser field begins to breakdown as intensities approach I_a. At these intensities the Coulomb field felt by electrons becomes warped by the strong laser field. Keldysh devised a parameter in 1965 that separated the regimes of tunneling and multiphoton ionization. This parameter is based on the laser intensity and ionization energy expressed as follows:

$$\gamma = \omega_L \sqrt{\frac{2E_{ion}}{I_L}}, \tag{2.42}$$

where I_L is the laser intensity. For $\gamma > 1$ mutiphoton ionization dominates (see Fig. 2.2 and for $\gamma < 1$ tunneling effects become pronounced. $\gamma > 1$ corresponds to weak laser fields and short laser wavelengths (high laser frequencies). The regimes of tunneling ionization along with above the barrier ionization are expressed in Figure 2.3.

These two phenomena are made possible by the laser's electric field modifying the electrostatic field of the atom so as to lower its potential well bellow the binding energy of the electron. This allows it to tunnel through the barrier at a fixed probability. If the potential well is warped even lower then over-the-barrier ionization can take place where electrons will

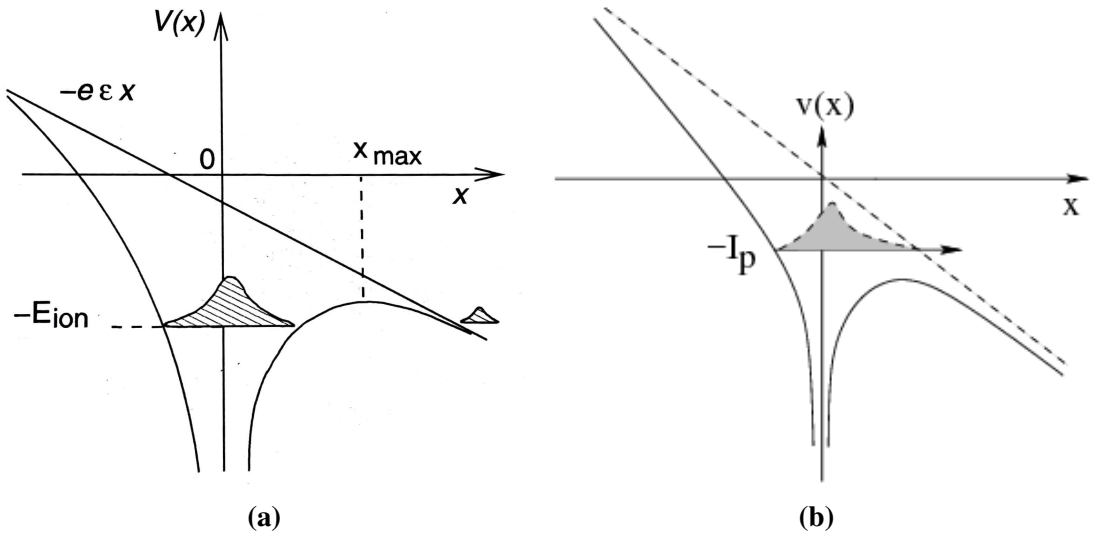

Figure 2.3. a) Schematic picture of tunneling or barrier-supression ionization by a strong external field. Adapted from P. Gibbon [13]. b) Schematic of over-the-barrier ionization. Adapted from Miguel [24]

spontaneously escape.

2.3 Plasma Mirrors

The CPA technique has pushed the laser industry forward in terms of achievable intensities at the pico and femto second regime. However as it has grown the intensity of the main pulse so to have the intensities of the pre-pulse and pedestal. A typical temporal beam profile consisting of the main pulse, pedestal and pre-pulse can be seen in Figure 2.4. These pedestals and pre-pulses cause issues when they ionize targets prematurely and, if the pre-pulse duration is long enough, hydrodynamically expand before the main pulse arrives. This changes the density profile reducing its steepness (typical of a solid) and changing the way in which the laser interacts with the target. This leads to uncertainty in the condition of the target when the main pulse of the laser arrives greatly complicating the process of understanding the physics behind the interaction. Furthermore, in the case of commercial processes where a reproducible phenomena is needed, the uncertainty of conditions produced by this laser pre-pulse and/or pedestal is unacceptable. These

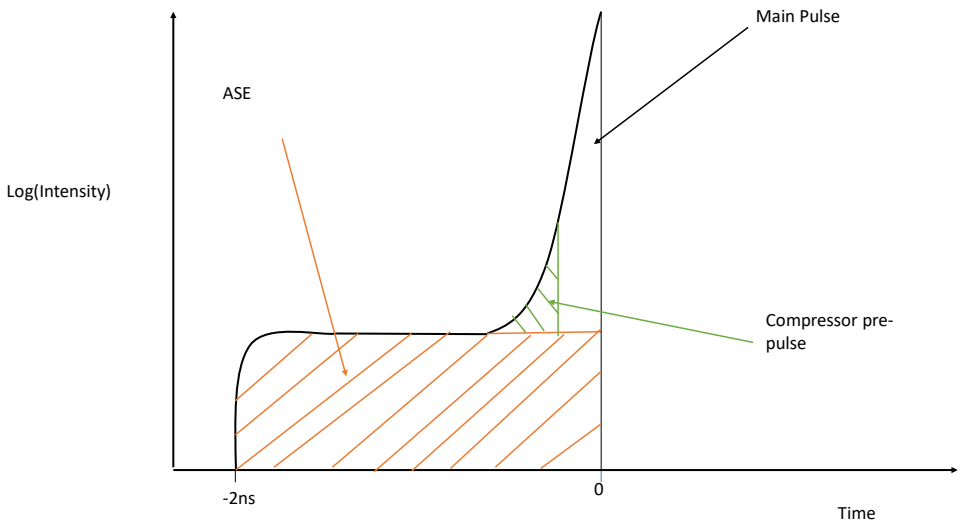

Figure 2.4. Sketch showing basic structure of a CPA laser pulse

issues persist in the experimental side as well which can be most clearly seen in experiments utilizing thin targets [17, 38] or targets with fine structures [31] on them.

As a result, plasma mirrors have been developed as a means to reduce the laser pre-pulse and/or predestal. This is referred to as an enhancement of laser contrast, where contrast is the ratio of the laser's peak intensity to the current intensity. To improve laser contrast, plasma mirrors have found widespread appeal as intensities as low as $10^8 - 10^9$ Wcm^{-2} have been seen to affect laser target interactions [38, 2]. Plasma mirrors operate by being placed before the laser's focal point where intensity/fluence are be low the ionization/damage threshold allowing up to 99.7% transmission [36]. Once the pre-pulse begins transitioning to the main pulse, the intensity rises on the surface of the plasma mirror high enough to rapidly ionize it via collisional ionization and multiphoton ionization [29] (if it is p-polarized resonant absorption also plays a part [35]). This quickly reaches the plasma's n_c at which point the laser can no longer propagate and the main pulse is reflected [18] as seen in Figure 2.5.

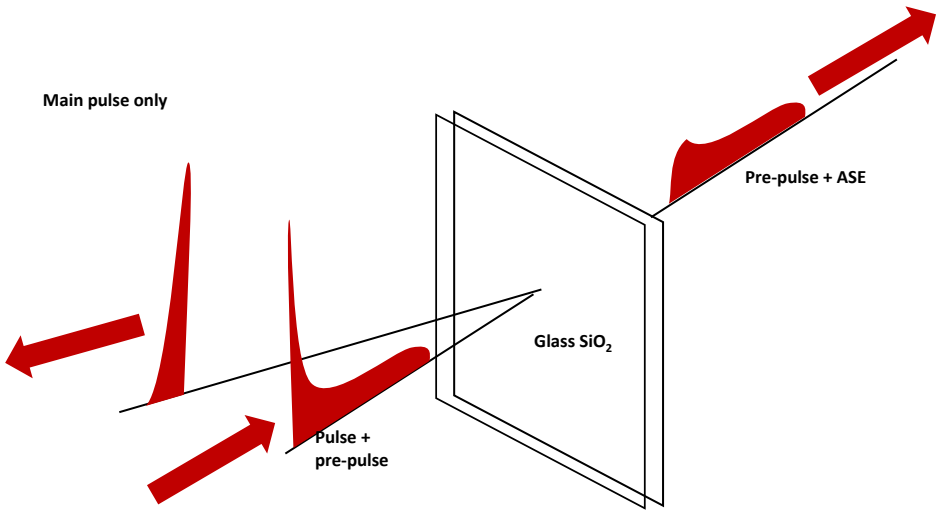

Figure 2.5. Sketch showing basic operation of a plasma mirror

2.3.1 Key Plasma Mirror Experimental Findings Thus Far

The pulse cleaning properties of a plasma mirror is particularly useful in femtosecond lasers as their high intensity (typically $> 10^{18} W cm^{-2}$) has an associated high intensity pre-pulse making targets more susceptible to pre-ionization. Since its inception in the 1990's [19, 15] work has been done to characterise its performance under varying conditions. G. Doumy *et al* [10] tested plasma mirrors on the LUCA laser with pulse durations of 60 fs for best compression and pulse chirped up to 4 ps. These results were used to benchmark their models for satisfactory usage conditions for a single plasma mirror and potential usage of a double plasma mirror if further contrast improvement is needed. This is plotted in Figure 2.6.They found that a single plasma mirror could enhance laser contrast by two orders of magnitude and that the plasma mirror also acts as a low-pass spatial filter smoothing the sharp edges in the near field. Using their method of chirping the signal it was seen that past 5 ps significant distortion to the wavefront became unavoidable.

In scenarios where further contrast enhancement is needed the double plasma mirror has been experimentally tested for viability [36, 23]. An example of a double plasma mirror setup

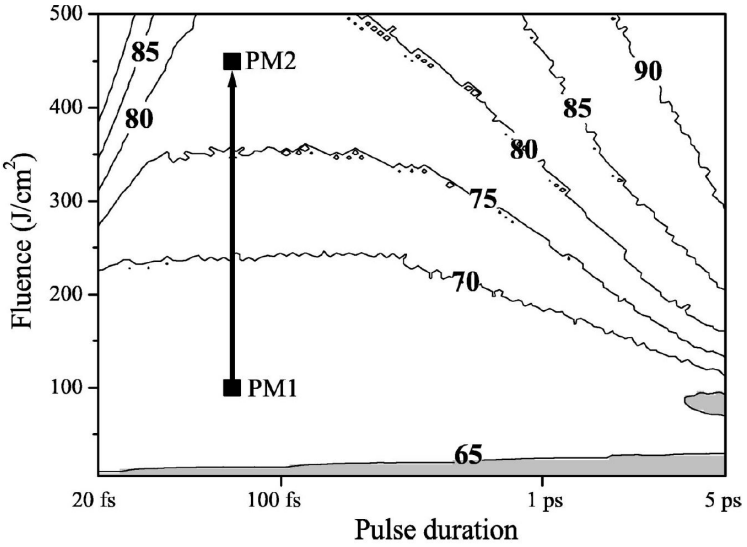

Figure 2.6. Reflectivity of the PM at the maximum of the laser pulse, as a function of the duration and fluence of the incident pulse. The area where the PM can be considered to trigger (reflectivity $> 65\%$) appears in white. The two points PM1 and PM2 show the typical fluences that could be used in a two-PM system, allowing contrast improvements by several 10^4. Taken from G. Doumy *et al* [10]

is seen in Figure 2.7 where two plasma plasma mirrors are setup before final focusing by Lévy *et al* [23]. Using two parabolas the the beam is focused between the two plasma mirrors and then subsequently re-collimated by the second parabola past the second plasma mirror. This contrast-enhanced beam is then sent off for final focusing allowing greater flexibility in the chamber. Three positions of the laser focus between the plasma mirrors were tested and it was found the center gave the best energy transmission. The results found that a double plasma mirror behaves as a single plasma mirror squared meaning SPM gave 10^2 contrast enhancement with 70% relfectivity and DPM gave 10^4 contrast enhancement with 50% reflectivity.

Reflectivity of a single plasma mirror has been well studied in the femtosecond regime by researches such as Ziener *et al* [41] and Scott *et al* [32]. Ziener (2002) did an extensive characterization by varying the intensity incident on the plasma mirror by either adjusting spot size via focus or by changing the laser energy. Varied angles of incidence along with two pulse durations (90 and 500 fs) were tested and in the end a maximum of 80% reflectivity was found.

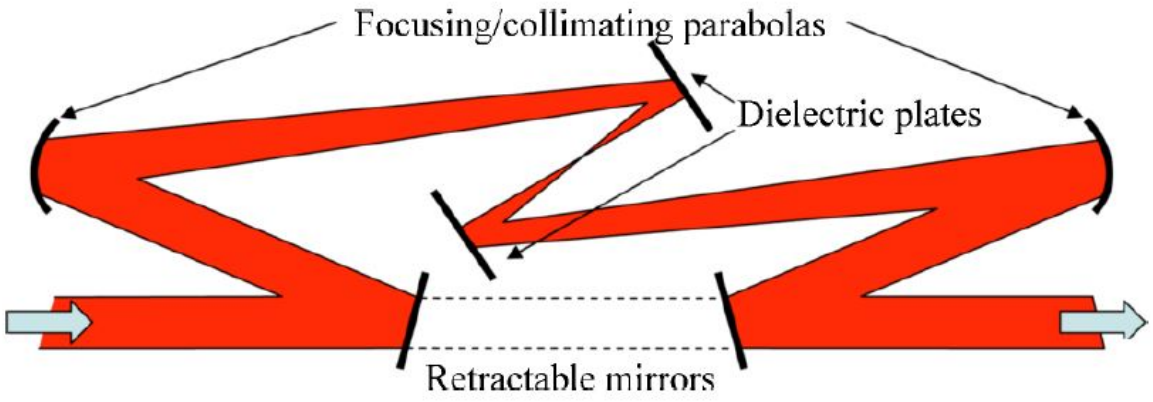

Figure 2.7. Experimental setup for the DPM (the laser comes from the left). Taken from Lévy *et al* [10]

The reflectivity response appeared to be bell shaped beginning at 10^{14} Wcm^{-2} corresponding to the triggering of the plasma mirror and falling off once intensity was pushed past 10^{16} Wcm^{-2}. This level of reflectivity remained the norm until Scott in 2015 utilized a double pulse system to ionize the plasma mirror several picoseconds before the main pulse arrived. This allowed a reflectivity of 96% to be achieved with a 3 ps inter-pulse delay.

As the understanding of plasma mirrors improves attempts to expand their utilization occurs. For high repetition experiments both liquid crystal [30] and rotating tape-based [33] plasma mirrors have been experimentally tested. The liquid crystal plasma mirror operated by injecting less than 10 μL of 4-octyl-4'-cyanobiphenyl (8CB) onto a smooth plate which a whiper spreads the solution to an optimal thickness of 270 nm. This achieved a reflectance of 75% while being automatic once setup due to the crystals vapour pressure being around 10^{-6} Torr. The tape plasma mirrors operated by using a device which Mylar tape to act as the plasma mirror. This process was done at a rate of 0.8 Hz and achieved a reflectivity of 74.8%.

The last usage of plasma mirrors studied is in fact what pertains most relevantly to this thesis. This is the study of curved plasma mirrors as disposable focusing optics. This was first done M. Nakatsutsumi [27] and A. Kon [20] in 2010. At Laboratoire pour l'Utilisation des Lasers Intenses (LULI) the experiment was carried out using elipsoidal plasma mirrors to reduce

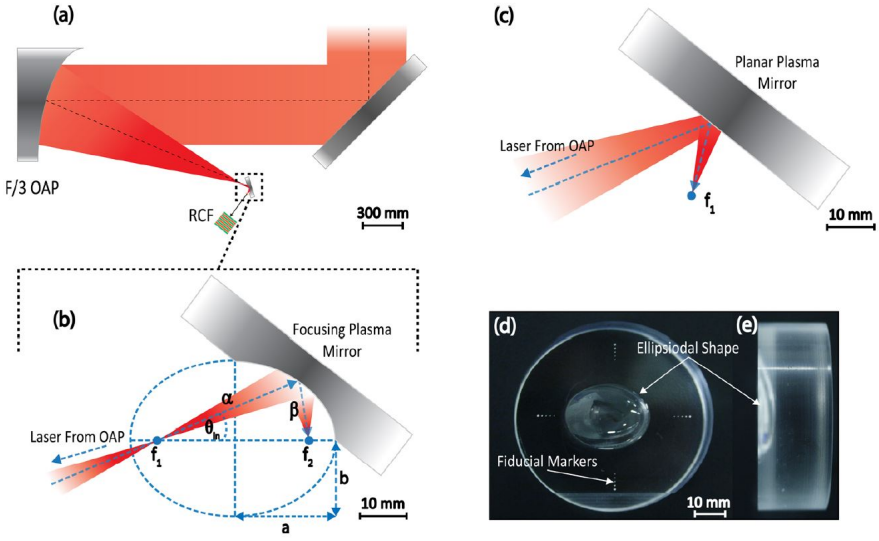

Figure 2.8. Schematic diagrams showing: (a) the overall optical set-up in the Vulcan target chamber; (b) the operation of the ellipsoidal focusing plasma mirror, where the incoming laser is focused by a conventional OAP to position f_1 and the FPM focuses the beam to position f_2, with magnification given by β/α; (c) the operation of a reference planar plasma mirror. (d) and (e) Photographs of the manufactured FPM optic showing: (d) the front surface and (e) a side view, demonstrating the ellipsoidal structure. The fiducial markers highlighted are used for alignment of the optic. Taken from Wilson *et al* [40]

the spot size of the focal spot. This would lead to an increase in achievable intensity beyond the 4.5×10^{18} Wcm^{-2} currently attainable by the 4.4 ± 0.5 μm FWHM spot on LULI. The first foci of the ellipsoidal plasma mirror coincides with the off axis parabola focus where the beam is relays the off axis parabola focus to the second foci of the elipsoidal plasma mirror. This changes the f number from $f/2.7$ to $f/0.4$ allowing for a magnification of 0.2. While energy is lost due to effects such as reflectivity, the reduction of spot size offsets these leasing to an enhancement factor of 8.4 (5^2 (spot size reduction) $\times$ $4.4^2/3^2$ (spatial filtering effect) $\times$ 0.3 (reflectivity) $\times$ 17/27 (encircled energy)). Following this, Wilson *et al* [39, 40] designed and tested ellipsoidal plasma mirrors for use on the Vulcan petawatt laser at the Rutherford Appleton Laboratory in the United Kingdom. The schematic of the setup for the experiment can be seen in Figure 2.8.

Their team found that reflectivity compared to a flat mirror was around 20% lower (65% for flat) with an enhancement of 3.6 to intensity when considering the reflectivity and encircled

energy. It was also found that the focal spot quality was highly sensitive to misalignments with a reduction of proton energy produced from an aluminum foil target by around 50%.

The summary of key experiments leads to the motivation behind this thesis.High intensity lasers continue to allow researchers to uncover new understandings in the study of matter in extreme conditions of pressure and temperature. This includes laboratory astrophysics [22, 26], warm dense matter [34, 11] and laser-driven particle acceleration [28, 4]. To continue probing ever newer conditions of matter, lasers must reach higher intensities and energies. However as plasma mirrors have been studied to combat this issue along with the problems which arise from CPA, these studies have remained focused in the femtosecond regime. The primary reason for this is the fact that once the plasma is created on the surface of the mirror it begins to expand and in the picosecond regime hydrodynamic expansion can cause significant distortions. However, these distortions have not been characterized in the 10's of picoseconds to determine beam quality. Further motivation comes from the need of not only high intensity but higher laser energies at these intensities whcih femtosecond lasers cannot come close to providing in comparison to picosecond beams. An example of this is the Advanced Radiographic Capability (ARC) laser [7] on the National Ignition Facility (NIF) as a x-ray backlighter for inertial confinement fusion experiments as the yield of x-rays scales favourably with laser intensity and energy [6, 37]. This all leads to the need for disposable focusing optics to be used on high energy picosecond lasers and the experiment below is the first step into this realization. It characterizes the focal spot quality for flat plasma mirrors and aluminum coated mirrors up to 20 picoseconds. It is the first step before moving onto curved mirrors which adds additional complications.

Chapter 3

Experimental Methods for picosecond pulses on Al coated and uncoated plasma mirrors

The experiment was carried out at the Compact Multipulse Terawatt (COMET) tabletop laser at the Jupiter Laser Facility (JLF) in Lawrence Livermore National Laboratory (LLNL). The system is a hybrid chirped-pulse amplification laser consisting of a Ti-sapphire oscillator and a regenerative amplifier tuned to 1053 nm allowing energies from $\sim$ 0.1 J to 10 J. Pulse durations ranged from half a picosecond to 20 picoseconds.

3.1 Experimental Setup and Image Processing

The laser beam was 8" off the bread board and all optics were set up with this in mind. Following the orientation of the schematic show in Figure 3.1, the laser pulse entered from the left side of the chamber and interacted with a mirror placed at 45 the laser's incident angle. The mirror transmitted approximately 1% of the pre-focused pulse onto a high-density plastic. This gave a near field which was imaged by a 12-bit Basler ACE CCD through a window of the chamber. The near field imaged here allowed for an energy measurement each shot, laser alignment and laser stability checks. The reflected portion of the pulse was then again reflected off of a mirror onto a $f/3$ parabola. The plasma mirror was placed 1 mm toward the parabola from the laser focus with an incident angle of 18 magnetic base along with x-y-z motorized

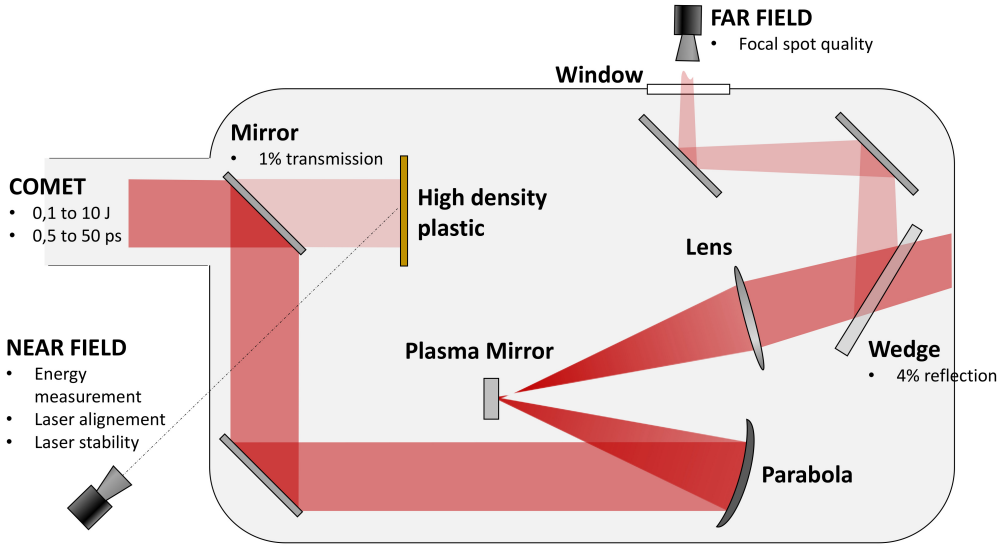

Figure 3.1. Schematic of experimental layout used to measure the far field after interacting with a plasma mirror.

translation stages were used to mount the plasma mirror to allow for initial alignment. Alignment of the plasma mirror was done with two of the translation stages' axes of movement being perpendicular to the incident beam. This allowed for the adjustment of the plasma mirror in vacuum without affecting focus, permitting multiple shots ($\sim$ 30 shots) before the need to bring the chamber to air. This is also a result of the laser damaging only a tiny spot on the mirror per shot ($\sim$ 2 mm wide).

Placed after the plasma mirror was a $f/2.3$ lens used to magnify the image by 10. After interacting with the lens, the beam hit a wedge to reduce the intensity by $\sim 96\%$. The now reduced beam hit two mirrors used to guide the beam outside a window onto the 12-bit Basler ACE CCD setup on the optical table outside the chamber with optical densities placed to protect the equipment. Also setup on the optical breadboard outside the chamber was an alignment system for the plasma mirrors. x-y-z translation stages and a magnetic base were setup based on the primary alignment done inside the chamber. Cross hairs were used to make sure alignment was correct and whenever the need arose to change the mirror inside the target chamber we were able to swap it out easily using the magnetic base.

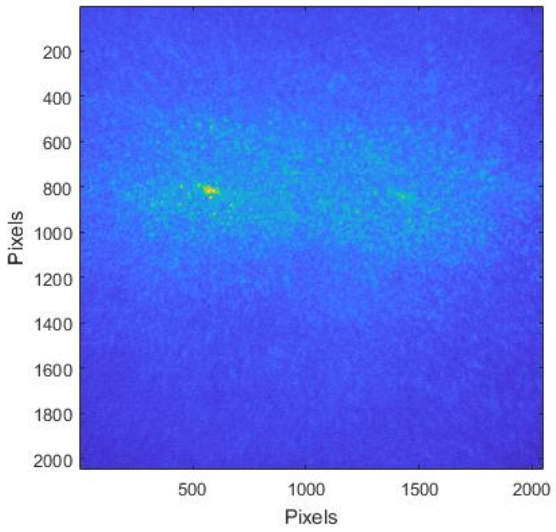

Figure 3.2. Example image of the raw data showing the far field and its reflection due to a window.

All images were saved and analysed using MATLAB. The optical densities used, pulse durations, energies and shot numbers for each shot as well as the target material were recorded. The code then processed the images in one of three ways:

1. Weighted Center
2. Gaussian Fitting
3. Manual Selection

The best method was chosen based on how well it was able to select the center of the far field. Firstly, the image was read and corrected for the optical density used on that particular shot (taken from the word document). This produced an image as seen in Figure 3.2.

As can be seen in Figure 3.2, there are two far field spots present. The one on the right is due to a reflection created by the window and as such is typically disregarded for the analysis. For the first method cropped the image to remove the reflection and then found the pixel with the highest value. This corresponded to the point of highest intensity. A square of sides 402 pixels was drawn around the point of highest intensity and then the weighted center was found

using the points within the sphere. This was done to remove influences from abnormalities that were clearly unrelated to the center point. The second method broke the image into two separate vectors by summing the matrix in either dimension. This lead to a column vector containing values summed in the x direction and row vector containing values summed in the y direction. These were then plotted and each fitted with a Gaussian function to extract the coordinates of the center of the far field. This coordinate corresponded to the center point of the gaussians. Lastly, the third method was utilized when the first two did not do an acceptable job of finding the far field center. Here the center of the focal spot was manually selected based on sight and checked using the fitting functions that assume a perfect focal spot (gaussian).

Once the center of the far field is found using one of the three methods, all data processing that follows is the same. The average radial profile was found summing the values for each radius and dividing it by the number of pixels that were summed for that point. This was then plotted as seen in Figure 3.3.

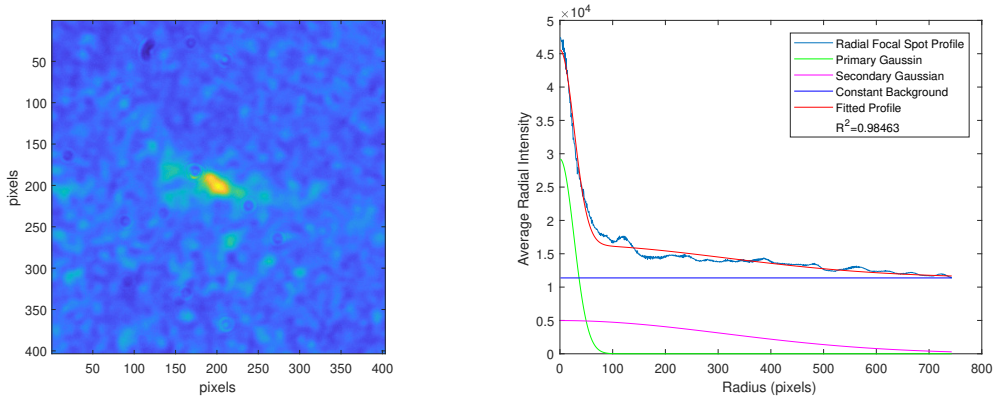

(a) Al: 9.95 J @20 ps **(b)** Al: 9.95 J @20 ps

Figure 3.3. a) Figure showing the far field for a shot on Al coated mirror at a long pulse duration and high energy. b) Plot showing the average radial profile for the same shot on Al coated target shown in a) with the primary gaussian, secondary gaussian and constant background that the profile was fitted to.

The average radial profile was subsequently fit by the sum of a constant background and two gaussians named primary and secondary gaussian. The two gaussian fits were constrained so that the primary gaussian is narrow with a high peak and the secondary gaussian is wide with

a lower peak. This was done so that the primary gaussian represents the 'ideal' focal spot which is a narrow spot with high intensity contained within. Alternatively, the secondary gaussian is a measure of the deterioration of the ideal focal spot as de-focusing occurs and the energy becomes spread over a larger area. This was used to calculate the energy enclosed fraction by integrating the two gaussians to find the area under their respective curves and dividing the area of the primary gaussian by the sum of the area of both gaussians.

The average radial profile was then background subtracted and cumulatively summed. This allowed for the determination of the 50% half width half maximum (50% HWHM) which is the width of the focal spot that contains half the energy. This also provided a metric in which to measure the accuracy of the background subtraction as if the background was accurately removed the normalized cumulative energy would end at 1 in a perfect case.

Chapter 4, in part is currently being prepared for submission for publication of the material. Brandon Edghill, Pierre Forestier-Colleoni, Jaebum Park, Alexander Rubenchik, Farhat N. Beg and Tammy Ma. The thesis author was the primary investigator and author of this material.

Chapter 4

Results for SiO_2 and Aluminum Coated Flat Mirrors

The first data to be analysed was the reference far field. This was captured using the pre-amplified beam from the laser bay which can be seen in Figure 4.1(a). It's half-width-half-maximum was then compared to the HWHM of the primary gaussian for the shots on SiO_2 and Al mirrors shown in Figure 4.2(a) and 4.2(b). All sizes were subsequently normalised by the primary gaussian's HWHM of the reference far field as the far field is a measure of divergence. This provides a metric to better understand the changes of the laser pulse as the divergence here captures both the change in size and the change in energy distribution with respect to the original. The added benefit is that the far field can be recorded at almost any distance (once greater than a few rayleigh lengths) after the interaction. The HWHM of the primary gaussian remains relatively unchanged with 0.69 ± 0.2 for SiO_2 and 1.03 ± 0.25 for Al both normalised to the reference far field where the error is the standard deviation of the averaged shots spread across the different laser conditions. This means any variation seen in the 50% HWHM comes down to the intensity and energy of the primary and secondary gaussian more so than their widths. Another point of interest is the SiO2 having a smaller primary gaussian than the reference gaussian. The cause of this is currently unknown but may be related to the SiO_2's strong scaling with multiphoton ionization (scales with I_{laser}^{8}) causing a focusing effect on the Far Field as it is not the actual focal spot being observed. In fact, this effect becomes more pronounced as the

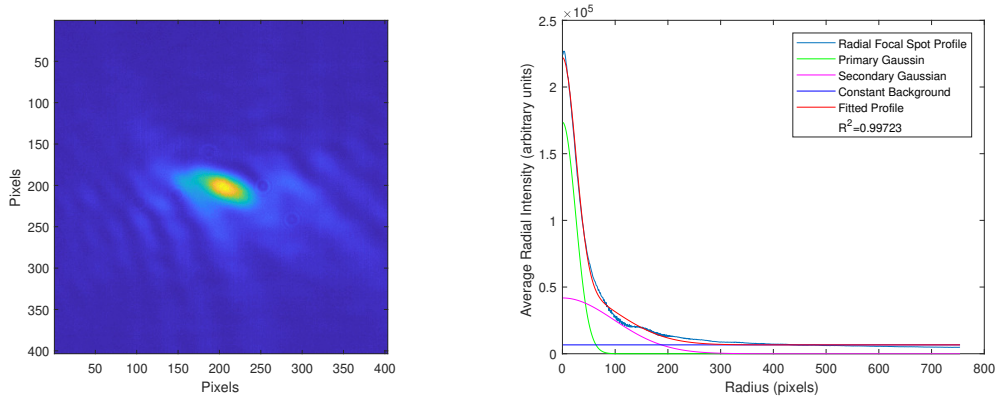

(a) **(b)**

Figure 4.1. (a) Raw image of the far field for the reference beam by using the pre-amplified beam.(b)Plot showing the refernce beam's average radial profile and accompanying fit.

pulse duration increases as the smallest primary gaussians recorded are for the 15 and 20 ps pulse shots. It may also be due to the spot degrading and only having a small hot spot surrounded by a diffuse spot.

Looking at the example raw data for the shots on SiO_2 and Al seen in Figure 4.3 the overarching story of Aluminum holding up better to more extreme conditions begins to present itself. These shots were taken under the same conditions at the longer pulse durations that are of key interest. Figure 4.3(a) shows a good quality focal spot with little spread. Comparing it to the shot on SiO_2 shown in Figure 4.3(b) which has a completely destroyed focal spot with diffuse hot spots spread throughout the image shows qualitatively that Al coated mirrors hold up better under higher energies and longer pulse durations.

The data was then quantitatively compared using the 50% HWHM as shown in Figure 4.4. Here the 50% HWHM is comapred to the intensity on the surface of the plasma mirror and is separated based on pulse duration. The error bars were found via a combination of calibration uncertainty and fitting parameters. This was done by propagating the errors associated with how well the data was fit, the error for energy calibration and the spatial error associated with the CCD imaging. Both materials were seen to have similar 50% HWHM widths within the same intensity range of 10^{13} to 10^{14} Wcm^{-2} with a greater spread for the Al coated mirrors. The

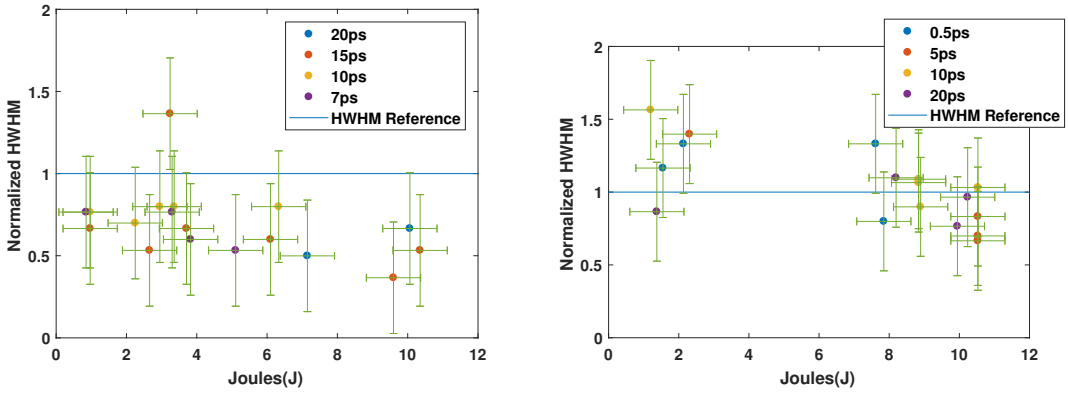

(a) SiO_2 **(b)** Al

Figure 4.2. (a) Plot comparing the half-width-half-maximum for the different shots on the SiO_2 plasma mirroir.(b) Plot comparing the half-width-half-maximum for the different shots on the Al coated plasma mirroir.

SiO_2 50% HWHM is seen to increase with increasing laser intensity for pulse durations above 7 ps. Though there are not enough data points at 20 ps to definitively say the trend continues at this pulse duration, the limited data points under this condition do not suggest otherwise. Furthermore,the longer the pulse duration the greater effect intensity appears to have on the 50% HWHM. As stated earlier this is interesting due to the relatively similar primary gaussian widths, indicating that most of the change is due to intensity and energy contained changes in the two gaussians. This also pertains to the following analysis of the energy enclosed within the primary gaussian which is shown in Figure 4.5.

Figure 4.5 shows further focal spot degradation in its comparison of the energy fraction enclosed in the primary gaussian and how it varies with respect to laser energy. This provides additional insight into focal spot quality as even if the width containing half the energy shrinks, if the energy contained within the high intensity primary gaussian is low then the peak achievable laser intensity on target will be trivial. Figure 4.5(a) shows SiO_2's enclosed energy fraction depreciating as laser energy increases, falling from 0.5 to $\sim$ 0.125. However, Figure 4.5(b) shows Al maintain an average enclosed energy fraction of 0.287 with no obvious decreasing trend. Here the error range is more significant as the enclosed energy takes into account the HWHM

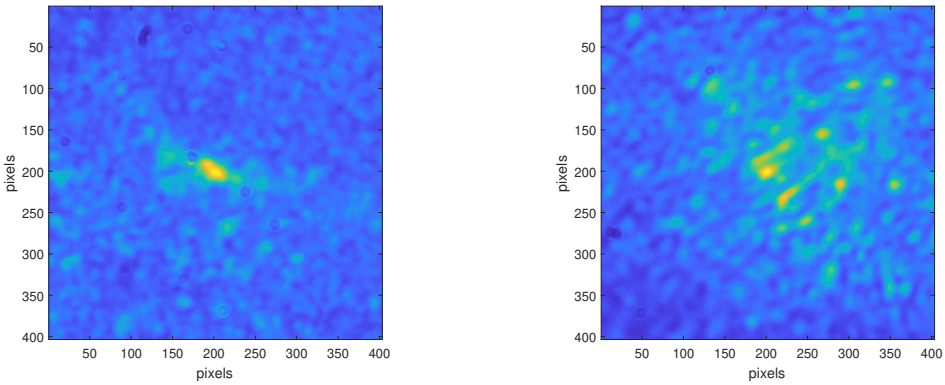

(a) Al: 9.95 J @20 ps **(b)** SiO_2: 10.06 J @ 20 ps

Figure 4.3. (a) and (b) Far Field images of Al coated mirror and SiO_2, respectively, at similar conditions of high energy and long pulse duration.

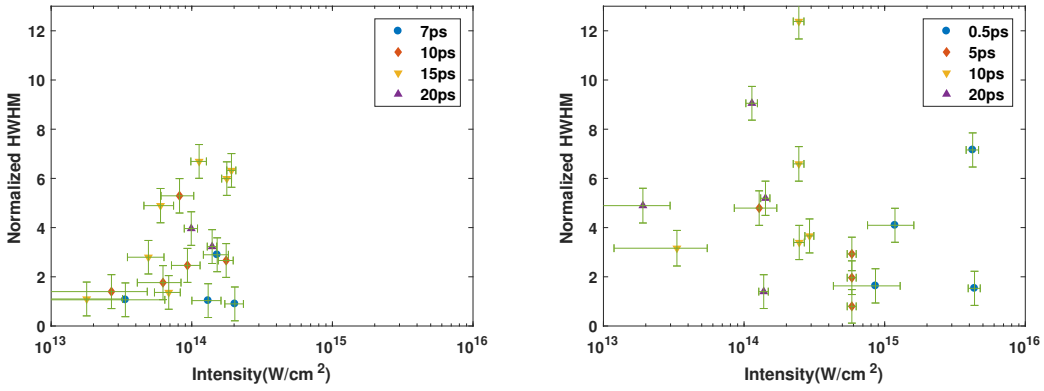

(a) **(b)**

Figure 4.4. (a) Plot of the 50% HWHM for SiO_2 against intensity incident on the plasma mirror. (b) Plot of the 50% HWHM for Al coated mirror against intensity incident on the plasma mirror

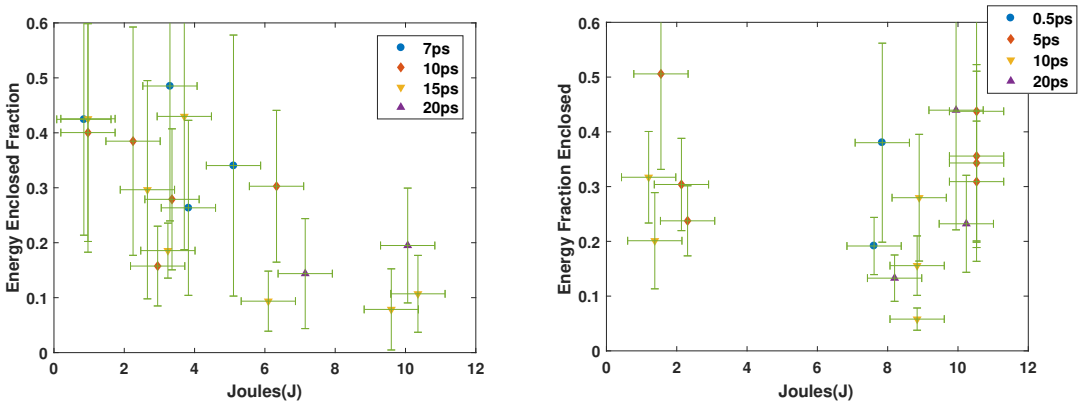

(a) **(b)**

Figure 4.5. (a) Plot of the fraction of energy contained within the primary gaussian against laser energy for SiO_2.(b)Plot of the fraction of energy contained within the primary gaussian against laser energy for Al.

of the primary gaussian where errors become less trivial due to the significantly smaller size of the primary gaussian compared to the 50% HWHM. It is important to note that Al still shows a significant spread similar to what was seen in Fig. 4.4(b). This may be due to the intrinsic properties of a plasma mirror. The ionization mechanism for SiO_2 and Al are different as one is a semiconductor and one is a metal. The SiO_2 is frequently used as the ionization is proportional to the I_{laser}^{8}. This means that the critical surface of the plasma mirror is not very sensitive to the near field of the laser (plasma mirror position corresponds to the laser near field). On the other hand, the Al interaction is linear. This means that the critical surface of the plasma is directly affected by the spatial fluctuations of the laser near field. This could lead to focusing and defocusing of the laser. Unfortunately, the regime of interaction (ps scale laser) is unsuitable for simulation to demonstrate this as PIC codes do not simulate resonance absorption and hydrodynamic codes are best suited for nanosecond pulse durations. However, with this in mind, Al still appears to maintain focal spot quality better than SiO_2 at longer pulse durations and higher energies.

Chapter 5, in part is currently being prepared for submission for publication of the material. Brandon Edghill, Pierre Forestier-Colleoni, Jaebum Park, Alexander Rubenchik, Farhat N. Beg and Tammy Ma. The thesis author was the primary investigator and author of this

material.

Summary

To summarize the findings, the focal spot quality for a multipicosecond beam was observed and findings for SiO_2 and Al coated mirrors were compared for possible applicability. It was seen that for increasing intensities, in the range of 10^{13} to mid 10^{14}Wcm^{-2}, the traditional glass plasma mirror spot size containing half the energy gradually increased. Furthermore, the energy contained within the primary gaussian (high intensity peak) dropped to $\sim 1/5\ th$ when comparing laser shots at 1 and 10J respectively. The Aluminum coated mirrors seemed to follow no distinct trends and fluctuated around 25% enclosed energy while keeping their primary gaussian closest to the reference far field. These findings suggest that while plasma mirrors of either SiO_2 or Al both defocus the beam, the Al still maintains applicable amounts of energy within the main focus. This is a successful first step in showing the viability of plasma mirrors, coated/un-coated, as potential disposable focusing optics in the picosecond regime. By first studying flat mirrors in the transition regime between purely multiphoton ionization and hydrodynamic interaction with inverse bremsstrahlung and resonant absorption, their viability to be used/tested as focusing optics as well as their behaviour in this regime is shown without the additional complication of curved mirrors. For cases where contrast improvement is needed Al can be used to focus the beam after it interacts at a lower fluence with SiO_2. Unfortunately, simulation for interactions on the picosecond laser is not possible as the PIC code misses needed effects and hydrodynamic codes do not have the resolution to solve the initial state of the laser plasma interaction. This experiment has laid the groundwork for a future experiment using what has been learnt to test curved surfaces for picosecond pulses. This material dependence shows there is room for growth in plasma mirror study and a potential avenue of use as a focusing optic

on multipicosecond lasers with sufficiently good contrast such as ARC on the NIF.

Bibliography

[1] Alfred kastler - biographical. nobelprize.org. nobel media ab 2019. tue. 10 dec 2019. url=¡https://www.nobelprize.org/prizes/physics /1966/ kastler/biographical/¿.

[2] T. R. Boehly, Y. Fisher, D. D. Meyerhofer, W. Seka, J. M. Soures, and D. K. Bradley. The effect of optical prepulse on direct-drive inertial confinement fusion target performance. *Physics of Plasmas*, 8(1):231–237, 2001.

[3] F. Brunel. Not-so-resonant, resonant absorption. *Phys. Rev. Lett.*, 59:52–55, Jul 1987.

[4] Alexander Buck, Maria Nicolai, Karl Schmid, Chris M. S. Sears, Alexander Sävert, Julia M. Mikhailova, Ferenc Krausz, Malte C. Kaluza, and Laszlo Veisz. Real-time observation of laser-driven electron acceleration. *Nature Physics*, 7:543 EP –, Mar 2011.

[5] Francis Chen. *Introduction to Plasma Physics and Controlled Fusion*. Springer International Publishing, 2016.

[6] Hui Chen, M. R. Hermann, D. H. Kalantar, D. A. Martinez, P. Di Nicola, R. Tommasini, O. L. Landen, D. Alessi, M. Bowers, D. Browning, G. Brunton, T. Budge, J. Crane, J.-M. Di Nicola, T. Döppner, S. Dixit, G. Erbert, B. Fishler, J. Halpin, M. Hamamoto, J. Heebner, V. J. Hernandez, M. Hohenberger, D. Homoelle, J. Honig, W. Hsing, N. Izumi, S. Khan, K. LaFortune, J. Lawson, S. R. Nagel, R. A. Negres, L. Novikova, C. Orth, L. Pelz, M. Prantil, M. Rushford, M. Shaw, M. Sherlock, R. Sigurdsson, P. Wegner, C. Widmayer, G. J. Williams, W. Williams, P. Whitman, and S. Yang. High-energy (¿70 kev) x-ray conversion efficiency measurement on the arc laser at the national ignition facility. *Physics of Plasmas*, 24(3):033112, 2017.

[7] J K Crane, G Tietbohl, P Arnold, E S Bliss, C Boley, G Britten, G Brunton, W Clark, J W Dawson, S Fochs, R Hackel, C Haefner, J Halpin, J Heebner, M Henesian, M Hermann, J Hernandez, V Kanz, B McHale, J B McLeod, H Nguyen, H Phan, M Rushford, B Shaw, M Shverdin, R Sigurdsson, R Speck, C Stolz, D Trummer, J Wolfe, J N Wong, G C Siders, and C P J Barty. Progress on converting a NIF quad to eight, petawatt beams for advanced radiography. *Journal of Physics: Conference Series*, 244(3):032003, aug 2010.

[8] R. O Dendy. *Plasma physics : an introductory course*. Cambridge [England] ; New York : Cambridge University Press, 1993. Includes bibliographical references and index.

[9] N.G. Denisov. On a singularity of the field on an electromagnetic wave propagated in an inhomogeneous plasma. *JETP*, 7 1955.

[10] G. Doumy, F. Quéré, O. Gobert, M. Perdrix, Ph. Martin, P. Audebert, J. C. Gauthier, J.-P. Geindre, and T. Wittmann. Complete characterization of a plasma mirror for the production of high-contrast ultraintense laser pulses. *Phys. Rev. E*, 69:026402, Feb 2004.

[11] L. B. Fletcher, H. J. Lee, T. Döppner, E. Galtier, B. Nagler, P. Heimann, C. Fortmann, S. LePape, T. Ma, M. Millot, A. Pak, D. Turnbull, D. A. Chapman, D. O. Gericke, J. Vorberger, T. White, G. Gregori, M. Wei, B. Barbrel, R. W. Falcone, C.-C. Kao, H. Nuhn, J. Welch, U. Zastrau, P. Neumayer, J. B. Hastings, and S. H. Glenzer. Ultrabright x-ray laser scattering for dynamic warm dense matter physics. *Nature Photonics*, 9:274 EP –, Mar 2015. Article.

[12] P. Gibbon. Introduction to plasma physics, 2017.

[13] Paul Gibbon. *Short Pulse Laser Interactions with Matter*. PUBLISHED BY IMPERIAL COLLEGE PRESS AND DISTRIBUTED BY WORLD SCIENTIFIC PUBLISHING CO., 2005.

[14] V.L. Ginzburg. *The Propagation of Electromagnetic Waves in Plasmas.* Pergamon Press, 1964.

[15] David M. Gold, Howard Nathel, Paul Robert Bolton, William E. White, and Linn D. Van Woerkom. Prepulse suppression using a self-induced ultrashort pulse plasma mirror. In Hector A. Baldis, editor, *Short-Pulse High-Intensity Lasers and Applications*, volume 1413, pages 41 – 52. International Society for Optics and Photonics, SPIE, 1991.

[16] David J. Griffiths. *Introduction to electrodynamics*. Cambridge University Press, 2018.

[17] M. Kaluza, J. Schreiber, M. I. K. Santala, G. D. Tsakiris, K. Eidmann, J. Meyer-ter Vehn, and K. J. Witte. Influence of the laser prepulse on proton acceleration in thin-foil experiments. *Phys. Rev. Lett.*, 93:045003, Jul 2004.

[18] Henry C. Kapteyn, Margaret M. Murnane, Abraham Szoke, and Roger W. Falcone. Prepulse energy suppression for high-energy ultrashort pulses using self-induced plasma shuttering. *Opt. Lett.*, 16(7):490–492, Apr 1991.

[19] Henry C. Kapteyn, Margaret M. Murnane, Abraham Szoke, and Roger W. Falcone. Prepulse energy suppression for high-energy ultrashort pulses using self-induced plasma shuttering. *Opt. Lett.*, 16(7):490–492, Apr 1991.

[20] A Kon, M Nakatsutsumi, S Buffechoux, Z L Chen, J Fuchs, Z Jin, and R Kodama. Geometrical optimization of an ellipsoidal plasma mirror toward tight focusing of ultraintense laser pulse. *Journal of Physics: Conference Series*, 244(3):032008, aug 2010.

[21] W.L. Kruer. *The physics of laser plasma interactions*. Frontiers in physics. Addison-Wesley, 1988.

[22] N. L. Kugland, D. D. Ryutov, P.-Y. Chang, R. P. Drake, G. Fiksel, D. H. Froula, S. H. Glenzer, G. Gregori, M. Grosskopf, M. Koenig, Y. Kuramitsu, C. Kuranz, M. C. Levy, E. Liang, J. Meinecke, F. Miniati, T. Morita, A. Pelka, C. Plechaty, R. Presura, A. Ravasio, B. A. Remington, B. Reville, J. S. Ross, Y. Sakawa, A. Spitkovsky, H. Takabe, and H.-S. Park. Self-organized electromagnetic field structures in laser-produced counter-streaming plasmas. *Nature Physics*, 8:809 EP –, Sep 2012.

[23] Anna Lévy, Tiberio Ceccotti, Pascal D'Oliveira, Fabrice Réau, Michel Perdrix, Fabien Quéré, Pascal Monot, Michel Bougeard, Hervé Lagadec, Philippe Martin, Jean-Paul Geindre, and Patrick Audebert. Double plasma mirror for ultrahigh temporal contrast ultraintense laser pulses. *Opt. Lett.*, 32(3):310–312, Feb 2007.

[24] Miguel A. L. Marques and Eberhard K. U. Gross. Time-dependent density functional theory. *Annual review of physical chemistry*, 55:427–55, 2004.

[25] C.E. Max. Physics of laser fusion. vol. i. theory of the coronal plasma in laser-fusion targets. 12 1981.

[26] J. Meinecke, H. W. Doyle, F. Miniati, A. R. Bell, R. Bingham, R. Crowston, R. P. Drake, M. Fatenejad, M. Koenig, Y. Kuramitsu, C. C. Kuranz, D. Q. Lamb, D. Lee, M. J. MacDonald, C. D. Murphy, H.-S. Park, A. Pelka, A. Ravasio, Y. Sakawa, A. A. Schekochihin, A. Scopatz, P. Tzeferacos, W. C. Wan, N. C. Woolsey, R. Yurchak, B. Reville, and G. Gregori. Turbulent amplification of magnetic fields in laboratory laser-produced shock waves. *Nature Physics*, 10:520 EP –, Jun 2014.

[27] M. Nakatsutsumi, A. Kon, S. Buffechoux, P. Audebert, J. Fuchs, and R. Kodama. Fast focusing of short-pulse lasers by innovative plasma optics toward extreme intensity. *Opt. Lett.*, 35(13):2314–2316, Jul 2010.

[28] E. A. Peralta, K. Soong, R. J. England, E. R. Colby, Z. Wu, B. Montazeri, C. McGuinness, J. McNeur, K. J. Leedle, D. Walz, E. B. Sozer, B. Cowan, B. Schwartz, G. Travish, and R. L. Byer. Demonstration of electron acceleration in a laser-driven dielectric microstructure. *Nature*, 503:91 EP –, Nov 2013.

[29] M. D. Perry, B. C. Stuart, P. S. Banks, M. D. Feit, V. Yanovsky, and A. M. Rubenchik. Ultrashort-pulse laser machining of dielectric materials. *Journal of Applied Physics*, 85(9):6803–6810, 1999.

[30] P. L. Poole, A. Krygier, G. E. Cochran, P. S. Foster, G. G. Scott, L. A. Wilson, J. Bailey, N. Bourgeois, C. Hernandez-Gomez, D. Neely, P. P. Rajeev, R. R. Freeman, and D. W. Schumacher. Experiment and simulation of novel liquid crystal plasma mirrors for high contrast, intense laser pulses. *Scientific Reports*, 6(1), 8 2016.

[31] P. P. Rajeev, S. Kahaly, S. Bose, P. Prem Kiran, P. Taneja, P. Ayyub, and G. Ravindra Kumar. Nanostructures and enhanced absorption in intense laser interaction with matter: effect of laser prepulses, 2005.

[32] G G Scott, V Bagnoud, C Brabetz, R J Clarke, J S Green, R I Heathcote, H W Powell, B Zielbauer, T D Arber, P McKenna, and D Neely. Optimization of plasma mirror reflectivity and optical quality using double laser pulses. *New Journal of Physics*, 17(3):033027, mar 2015.

[33] T. Sokollik, S. Shiraishi, J. Osterhoff, E. Evans, A. J. Gonsalves, K. Nakamura, J. van Tilborg, C. Lin, C. Toth, and W. P. Leemans. Tape-drive based plasma mirror. *AIP Conference Proceedings*, 1299(1):233–237, 2010.

[34] P. Sperling, E. J. Gamboa, H. J. Lee, H. K. Chung, E. Galtier, Y. Omarbakiyeva, H. Reinholz, G. Röpke, U. Zastrau, J. Hastings, L. B. Fletcher, and S. H. Glenzer. Free-electron x-ray laser measurements of collisional-damped plasmons in isochorically heated warm dense matter. *Phys. Rev. Lett.*, 115:115001, Sep 2015.

[35] U. Teubner, J. Bergmann, B. van Wonterghem, F. P. Schäfer, and R. Sauerbrey. Angle-dependent x-ray emission and resonance absorption in a laser-produced plasma generated by a high intensity ultrashort pulse. *Phys. Rev. Lett.*, 70:794–797, Feb 1993.

[36] C Thaury, Fabien Quere, J P. Geindre, Anna Levy, Tiberio Ceccotti, P Monot, Michel Bougeard, F Reau, P D'Oliveira, Patrick Audebert, Robin Marjoribanks, and P H. Martin. Plasma mirrors for ultrahigh-intensity optics. *Nature Physics*, 3:424–429, 04 2007.

[37] R. Tommasini, C. Bailey, D. K. Bradley, M. Bowers, H. Chen, J. M. Di Nicola, P. Di Nicola, G. Gururangan, G. N. Hall, C. M. Hardy, D. Hargrove, M. Hermann, M. Hohenberger, J. P. Holder, W. Hsing, N. Izumi, D. Kalantar, S. Khan, J. Kroll, O. L. Landen, J. Lawson, D. Martinez, N. Masters, J. R. Nafziger, S. R. Nagel, A. Nikroo, J. Okui, D. Palmer, R. Sigurdsson, S. Vonhof, R. J. Wallace, and T. Zobrist. Short pulse, high resolution, backlighters for point projection high-energy radiography at the national ignition facility. *Physics of Plasmas*, 24(5):053104, 2017.

[38] K. B. Wharton, C. D. Boley, A. M. Komashko, A. M. Rubenchik, J. Zweiback, J. Crane, G. Hays, T. E. Cowan, and T. Ditmire. Effects of nonionizing prepulses in high-intensity laser-solid interactions. *Phys. Rev. E*, 64:025401, Jul 2001.

[39] R. Wilson, M. King, R. J. Gray, D. C. Carroll, R. J. Dance, C. Armstrong, S. J. Hawkes, R. J. Clarke, D. J. Robertson, D. Neely, and P. McKenna. Ellipsoidal plasma mirror focusing of high power laser pulses to ultra-high intensities. *Physics of Plasmas*, 23(3):033106, 2016.

[40] Robbie Wilson, Martin King, Ross Gray, David C. Carroll, Rachel Dance, Nicholas Butler, Chris Armstrong, Steve J. Hawkes, Robert J. Clarke, David J. Robertson, Cyril Bourgenot, David Neely, and Paul Mckenna. Development of focusing plasma mirrors for ultraintense laser-driven particle and radiation sources. *Quantum Beam Science*, 2:1, 01 2018.

[41] Ch. Ziener, P. S. Foster, E. J. Divall, C. J. Hooker, M. H. R. Hutchinson, A. J. Langley, and D. Neely. Specular reflectivity of plasma mirrors as a function of intensity, pulse duration, and angle of incidence. *Journal of Applied Physics*, 93(1):768–770, 2003.